

Cloud radar Doppler spectra in drizzling stratiform clouds:

1. Forward modeling and remote sensing applications

Pavlos Kollias,¹ Jasmine Rémillard,¹ Edward Luke,² and Wanda Szyrmer¹

Received 24 October 2010; revised 3 March 2011; accepted 20 April 2011; published 2 July 2011.

[1] Several aspects of spectral broadening and drizzle growth in shallow liquid clouds remain not well understood. Detailed, cloud-scale observations of microphysics and dynamics are essential to guide and evaluate corresponding modeling efforts. Profiling, millimeter-wavelength (cloud) radars can provide such observations. In particular, the first three moments of the recorded cloud radar Doppler spectra, the radar reflectivity, mean Doppler velocity, and spectrum width, are often used to retrieve cloud microphysical and dynamical properties. Such retrievals are subject to errors introduced by the assumptions made in the inversion process. Here, we introduce two additional morphological parameters of the radar Doppler spectrum, the skewness and kurtosis, in an effort to reduce the retrieval uncertainties. A forward model that emulates observed radar Doppler spectra is constructed and used to investigate these relationships. General, analytical relationships that relate the five radar observables to cloud and drizzle microphysical parameters and cloud turbulence are presented. The relationships are valid for cloud-only, cloud mixed with drizzle, and drizzle-only particles in the radar sampling volume and provide a seamless link between observations and cloud microphysics and dynamics. The sensitivity of the five observed parameters to the radar operational parameters such as signal-to-noise ratio and Doppler spectra velocity resolution are presented. The predicted values of the five observed radar parameters agree well with the output of the forward model. The novel use of the skewness of the radar Doppler spectrum as an early qualitative predictor of drizzle onset in clouds is introduced. It is found that skewness is a parameter very sensitive to early drizzle generation. In addition, the significance of the five parameters of the cloud radar Doppler spectrum for constraining drizzle microphysical retrievals is discussed.

Citation: Kollias, P., J. Rémillard, E. Luke, and W. Szyrmer (2011), Cloud radar Doppler spectra in drizzling stratiform clouds: 1. Forward modeling and remote sensing applications, *J. Geophys. Res.*, *116*, D13201, doi:10.1029/2010JD015237.

1. Introduction

[2] Low-level stratiform clouds have an important impact on the boundary layer dynamics and global climate [Bony and Dufresne, 2005]. Extensive sheets of stratus and stratocumulus clouds lie above the eastern boundary current upwelling regions over the world's oceans. These clouds affect the radiative budget through the reflection of solar radiation that cannot be compensated for by thermal emission trapping at such low altitudes [Randall *et al.*, 1984; Albrecht *et al.*, 1988]. The parameterization of marine stratus clouds in GCMs is a challenge of current concern, particularly the representation of drizzle. Drizzle is ubiquitous in marine stratocumulus [e.g., Serpetzoglou *et al.*, 2008]. Modeling

studies show the boundary layer thermodynamic structure and capping stratocumulus decks to be greatly influenced by drizzle [e.g., Nicholls, 1984; Ackerman *et al.*, 1993; Pincus and Baker, 1994; Stevens *et al.*, 1998; vanZanten and Stevens, 2005; Comstock *et al.*, 2007; Ackerman *et al.*, 2009].

[3] Millimeter-wavelength Doppler radars, often called cloud radars, are best suited for the study of cloud and drizzle properties in low-level stratiform clouds [e.g., Kollias *et al.*, 2007]. Due to their short wavelength, millimeter radars are capable of detecting small cloud droplets and, due to their narrow beam width (half a degree or better), can achieve high spatial resolution. In a profiling mode, the primary measurement of Doppler cloud radars is the radar Doppler spectrum that reports the full distribution of the return radar echo over a range of sampled Doppler velocities. Typically, the first three moments of the radar Doppler spectrum are reported and used in radar data analysis: the total back-scattered power to the radar (Z , zeroth moment), the mean Doppler velocity (V_D , first moment), and the Doppler spectrum width (σ_D , second moment, or standard deviation of the Doppler velocities).

¹Department of Atmospheric and Oceanic Sciences, McGill University, Montreal, Quebec, Canada.

²Atmospheric Sciences Division, Brookhaven National Laboratory, Upton, New York, USA.

[4] The potential of using Doppler spectra from profiling radars to retrieve dynamical and microphysical properties of clouds and precipitation has been considered since the early days of radar meteorology [e.g., *Rogers and Pilié*, 1962; *Battan*, 1964; *Caton*, 1966]. In the absence of air turbulence, the Doppler spectra velocity bins with significant atmospheric radar return can be used to retrieve particle size and their corresponding spectral power density can be used to retrieve particle number concentration. This relatively straightforward retrieval approach is challenged by air turbulence at different physical scales. Turbulence at scales smaller than the radar sampling volume adds a random vertical air motion contribution and smears the return radar power spectrum adding a turbulence broadening term (σ_t) to the observed Doppler spectrum width. In addition, the average vertical air motion (w_{air}) of the radar sampling volume adds a bias (offset) to the observed Doppler velocity and thus disrupts the one-to-one correspondence between the observed Doppler velocities and particle fall velocities. In a nutshell, the observed radar Doppler spectrum contains convoluted information about cloud microphysics and dynamics [e.g., *Luke et al.*, 2010] and inversion (deconvolution) from radar Doppler moments to cloud microphysics and dynamics is not straightforward and can lead to large uncertainties [e.g., *Atlas et al.*, 1973].

[5] Noteworthy, there are occasions where the deconvolution of the dynamical and microphysical effects can be facilitated by the scattering mechanism or the particularities of the particles' size distribution (PSD). For instance, wind profilers are sensitive to coherent scattering produced by inhomogeneities of the radio index of refraction [*Rogers et al.*, 1993; *Gage et al.*, 1994]. Therefore, the observed Doppler spectrum is sometimes composed of two distinct spectral peaks, one corresponding to echoes from turbulent air refractive index irregularities (Bragg scattering) and the other to precipitation particle backscattering (Rayleigh scattering). The turbulent (Bragg) peak denotes the vertical air motion (w_{air}) and its broadening contains information about the turbulence broadening (σ_t) of the PSD Doppler spectrum [*Wakasugi et al.*, 1986, 1987; *Williams et al.*, 1995; *Cifelli et al.*, 2000]. Another example is the use of Mie scattering signatures at 94 GHz in precipitation. In the Mie scattering regime, the backscattering cross section as a function of the raindrop diameter oscillates due to resonant electromagnetic multipoles effects. Under precipitating conditions at 94 GHz, these oscillations are apparent in the observed Doppler spectrum and can be used as reference points for the retrieval of the vertical air motion (w_{air}) and subsequently the PSD [*Lhermitte*, 1988; *Kollias et al.*, 2002; *Giangrande et al.*, 2010]. Finally, another example where the deconvolution of the microphysical and dynamical effects is assisted by the observations is the case of bimodal (well separated peaks) Doppler spectra, where one of the spectral peaks corresponds to liquid cloud droplets and the other to either drizzle or ice particles. In this case, the cloud droplets spectral peak can be used in a manner similar to the use of the Bragg spectral peak in wind profilers and thus infer the vertical air motion w_{air} and the turbulence broadening (σ_t) term [e.g., *Kollias et al.*, 2001; *Shupe et al.*, 2004].

[6] Despite the frequent observation of such "golden" bimodal radar Doppler spectra, their analysis can only provide a limited view of the complex microphysical and

dynamical feedbacks in stratus clouds. Furthermore, the wind profiler and Mie scattering approaches are not applicable in the case of drizzling stratiform clouds. Despite the aforementioned challenges, several retrieval techniques for the estimation of cloud and drizzle drop distributions based on the moments of the radar Doppler spectrum have been proposed [*Gossard*, 1994; *Gossard et al.*, 1997; *Frisch et al.*, 1995, 2002]. *Frisch et al.* [1995] used the first three moments of the radar Doppler spectrum in drizzling marine stratus clouds to retrieve the drizzle PSD (assumed to be lognormal). Given the number of unknown parameters, assumptions are required about the cloud dynamics in order to retrieve the drizzle PSD parameters and subsequent moments (e.g., water content, precipitation rate).

[7] In this paper, we introduce the skewness and kurtosis of the radar Doppler spectrum as additional observational parameters that can be used to improve the qualitative and quantitative retrieval of drizzle parameters in stratiform clouds. Using a comprehensive data set from continental and marine stratiform clouds we demonstrate that the measured skewness and kurtosis of the radar Doppler spectrum (shape parameters) can be related to the drizzle amount and PSD parameters in the radar resolution volume. Analytical expressions that relate the skewness and kurtosis of the Doppler spectrum for a variety of microphysical and dynamical conditions are presented and benchmarked against the observations. In addition, a radar Doppler spectrum simulator is described and used to further validate the proposed relationships. The simulator is also used to examine the sensitivity of the measured shape parameters to signal-to-noise conditions and radar Doppler spectra velocity resolution.

2. Background

2.1. Recording and Processing of Radar Doppler Spectra at the ARM Sites

[8] Observations from the cloud radars of the U.S. Department of Energy Atmospheric Radiation Measurement (ARM) program are used in this study. Two different cloud radar systems are used to collect observations from a continental and a marine site: the MilliMeter wavelength Cloud Radar (MMCR) at the ARM Southern Great Plains (SGP) site, and the W band ARM Cloud Radar (WACR) of the ARM Mobile Facility (AMF) at Graciosa Island in the Azores [*Moran et al.*, 1998; *Widener and Mead*, 2004]. The MMCR is a 35 GHz Doppler radar that cycles over four different sampling modes of the atmospheric column, and here we use observations from the boundary layer mode that provides high vertical resolution in the lower atmosphere [*Kollias et al.*, 2005]. Since 2004, radar Doppler spectra are continuously recorded using an optimum sampling strategy that aims to minimize the impact of turbulence and wind shear on the recorded Doppler spectrum and thus maintain significant microphysical signatures [*Kollias et al.*, 2007]. Six coherent averages are performed in the time domain to reduce the Nyquist velocity. One second integration is used and several spectra are averaged to achieve the final 256-point long radar Doppler spectrum. The WACR is a 95 GHz Doppler radar that makes observations in alternating copolar and cross-polar modes, and here only observations from the copolar channel are used. No coherent averaging is performed and a very large number of spectral averages are used to estimate a

Table 1. Relevant Operating Characteristics of the Cloud Radars

Radar Parameter	SGP MMCR	GRW WACR
Frequency (GHz)/Wavelength (mm)	35/8.6	95/3.1
Antenna 3dB beam width (degrees)	0.19°	0.19°
Mode	BL	copolar
Vertical resolution (m)	45	42.86
Number of coherent averages	6	—
Number of spectral averages	10	80
Number of FFTs	256	256
Dwell time (s)	1.044	~2
Nyquist velocity (m/s)	5.27	7.885
Spectra velocity resolution (cm/s)	4.12	6.16
Sensitivity (dBZ)	-36 at 5 km	-35 at 10 km

256-point radar Doppler spectrum using 2 s signal integration. In both systems, the large number of averaged samples (MMCR ~ 15 k, WACR ~ 20 k) results in recorded Doppler spectra with little noise variance across the FFT. The radars characteristics relevant to this study are shown in Table 1.

[9] The postprocessing of the radar Doppler spectra starts with the objective determination of the noise floor using the method devised by *Hildebrand and Sekhon* [1974]. The average noise power spectral density is subtracted at all the FFT points. Subsequently, the Doppler velocity ranges that contain coherent atmospheric signal are identified. If a single spectral peak is observed, we estimate the first three

moments of the Doppler spectrum, and the skewness and kurtosis. If two or more spectral peaks are detected, we check if there is a spectral image due to I/Q amplitude and phase imbalance and remove it. Then, all the parameters are estimated for each spectral peak. Examples of radar Doppler spectra as recorded by the WACR at Graciosa Island are shown in Figures 1a and 1b. The cloud spectrum exhibits a weak spectral peak power with an approximate Gaussian distribution while the drizzle spectrum shows a strong, wide spectral peak with apparent non-Gaussian power distribution.

2.2. Forward Modeling of Radar Doppler Spectra

[10] A forward model was developed to simulate ARM cloud radar Doppler spectra for a variety of cloud and/or drizzle PSDs and turbulent conditions. The forward model can simulate Doppler spectra from cloud droplets alone, drizzle droplets alone and combinations of cloud and drizzle PSDs. The individual PSDs are all taken to be lognormal functions, which can be described by the following equation:

$$n(r) = \frac{N}{\sqrt{2\pi}\sigma_x r} \exp\left(-\frac{(\ln r - \ln r_o)^2}{2\sigma_x^2}\right), \quad (1)$$

where r is the particle radius, N is the total number of drops per unit volume, σ_x is the logarithmic width of the distribution, and r_o is the number median (hereafter median)

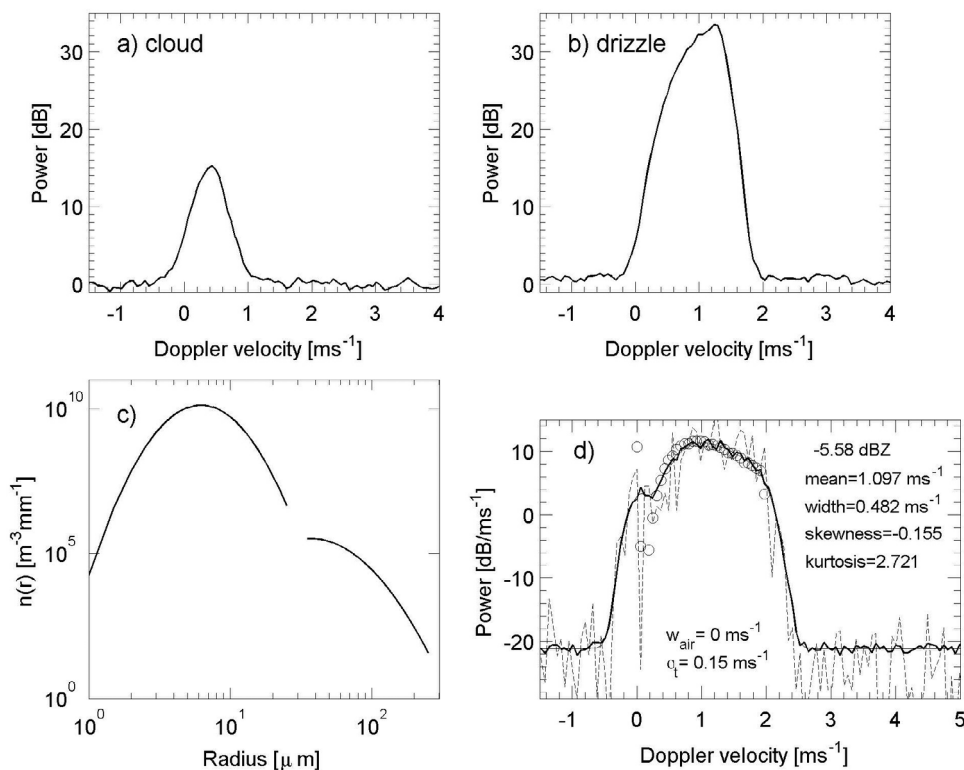


Figure 1. Example of W band Doppler spectra measured in the Azores from (a) cloud and (b) drizzle beneath cloud base, (c) example of input cloud and drizzle PSDs, and (d) the resulting simulated radar Doppler spectrum. The numbers on the right in Figure 1d are the computed values of various parameters (reflectivity, mean velocity, spectral width, skewness, and kurtosis) of the final spectrum (thick line). The circles represent the ideal quiet air spectrum (air characteristics are shown at the bottom); the thin solid line is the noise-free turbulent spectrum; the dashed line is one noisy spectrum; and the thick line is the averaged noisy spectrum.

radius [e.g., Frisch *et al.*, 1995]. The quantity $n(r)dr$ represents the number of particles found with a radius between r and $r + dr$. As in past studies [e.g., Frisch *et al.*, 1995; Miles *et al.*, 2000], the boundary between cloud droplets and drizzle drops is set at a radius of $25 \mu\text{m}$, although a small gap between the two PSDs is introduced in the simulator to avoid a discontinuity at the transition radius. Thus, the drizzle PSD has its lower bound at $35 \mu\text{m}$ radius, while its upper bound can be varied to a value smaller than $250 \mu\text{m}$ (droplets larger than $250 \mu\text{m}$ may present complications due to their scattering and attenuation properties, so the upper size bound is set accordingly). The cloud PSD has a minimum radius of $1 \mu\text{m}$ (lower limit of detection for most in situ instruments, and smaller droplets do not impact much anyway). Finally, the PSDs have a resolution of $0.5 \mu\text{m}$ in radius (see Figure 1c for an example).

[11] For each class of particle, a simple size-velocity relation is assumed. Cloud droplets are small enough that their fall velocity is in the Stokes regime: $V_f = cr^2$, with $c = 1.2 \times 10^8 \text{ m}^{-1}\text{s}^{-1}$ [Rogers and Yau, 1989]. On the other hand, a linear relationship is usually well representative of drizzle drops' fall speed, such that $V_f(r) = a \cdot r - b$, with $a = 8333 \text{ s}^{-1}$ and $b = 0.0833 \text{ ms}^{-1}$ [Frisch *et al.*, 1995]. Since the particles of interest are small enough to remain spherical, Mie theory is applied to compute their backscatter cross sections σ_b (mm^2). Thus, an ideal quiet air Doppler spectrum $S_Q(V_f)$ ($\text{mm}^6 \text{ m}^{-3} / \text{ms}^{-1}$) can be obtained using the following formula:

$$S_Q(V_f) = \frac{\lambda^4}{\pi^5 |K|^2} n(r) \sigma_b \frac{dr}{dV_f}, \quad (2)$$

where λ (mm) is the considered wavelength and $|K|^2$ is the refractive index factor. The result is then interpolated to the simulated Doppler radar velocity resolution.

[12] The dynamical contribution to the radar Doppler spectrum location and shape (radar sampling volume averaged vertical air motion and turbulence broadening) is considered next. The forward model assumes that cloud and drizzle particles in the radar sampling volume are equally affected by vertical air motion (same inertia). In addition, due to the narrow antenna beam width (Table 1) the horizontal wind broadening contribution is neglected. Thus, the radar sampling volume averaged vertical air motion causes a simple translation of the entire radar return power spectrum in the velocity space, while small-scale turbulence is parameterized by the convolution of a Gaussian function $g(V_f)$ having a prescribed width (σ_t) with the quiet air spectrum $S_Q(V_f)$ [e.g., Gossard, 1994]. The σ_t (ms^{-1}) parameter is the turbulent spectral broadening and can be related to the turbulent eddy dissipation rate ε ($\text{m}^2 \text{ s}^{-3}$) [e.g., Kollias *et al.*, 2001; O'Connor *et al.*, 2005]. The convolution operation on the quiet air Doppler spectrum and turbulence function is represented by the following expression:

$$S_t(V_f) = [S_Q * g](V_f) = \frac{1}{\sqrt{2\pi}\sigma_t} \int_{-V_N}^{V_N} S_Q(v) \exp\left[-\frac{(V_f - v)^2}{2\sigma_t^2}\right] dv, \quad (3)$$

$$S_w(V_f + w_{air}) = S_t(V_f), \quad (4)$$

where $S_t(V_f)$ is the radar Doppler spectrum resulting from the convolution of the turbulence function $g(V_f)$ with the quiet air Doppler spectrum $S_Q(V_f)$, with the integral covering all velocity bins of the simulated Doppler spectrum, and $S_w(V_f)$ is the radar Doppler spectrum after the vertical air motion w_{air} velocity shift.

[13] The next step is the addition of the radar receiver noise to the simulated Doppler spectrum. Using the radar constant of the simulated radar and the target range, the well-characterized ARM cloud radar receiver noise power P_N is converted from mWatts to $\text{mm}^6 \text{ m}^{-3}$. Noise has a white spectrum, causing its mean power to be independent of the frequency/velocity of the Doppler spectrum. Thus, the noise spectral density $P_{N,fft}$ ($\text{mm}^6 \text{ m}^{-3} / \text{ms}^{-1}$) is provided by the following expression:

$$P_{N,fft} \left(\frac{\text{mm}^6 \text{ m}^{-3}}{\text{ms}^{-1}} \right) = \frac{P_N}{N_{fft} \cdot \Delta\nu}, \quad (5)$$

where N_{fft} is the number of FFT points in the radar Doppler spectrum and $\Delta\nu$ is the spectral velocity resolution. Once the mean noise power density is estimated, we add a random fluctuation component following the method described by Zrnić [1975] and the spectral power density of the signal-plus-noise $P_{S+N,fft}$ is given by the expression:

$$P_{S+N,fft}(i) = -(S_w(i) + P_{N,fft}) \ln(x(i)), \text{ with } i = 1, \dots, N_{fft} \quad (6)$$

where x is a uniformly distributed random number between 0 and 1. Successive Doppler spectra are averaged (number of spectral averages, Table 1) to accurately emulate the noise in the recorded spectrum. Figure 1d illustrates the various spectra created at each step of the simulation process. Further analysis of the simulated spectra can now be done on the final Doppler spectrum the same way as for the measured spectra. Examples of the computed parameters are included in Figure 1d. Examples of radar Doppler spectra as recorded by the WACR at Graciosa Island are shown in Figures 1a and 1b.

3. Cloud and Drizzle Radar Doppler Moments

[14] Using the radar Doppler spectra forward model and simple scaling arguments, the first three cloud radar Doppler moments (e.g., the reflectivity factor Z , the mean Doppler velocity V_D and the spectral width σ_D) have been related to dynamical (w_{air} , ε) and microphysical (N , r_o , σ_x) parameters [e.g., Gossard, 1994; Frisch *et al.*, 1995]. Here, these relationships are expanded to include the skewness s_D and kurtosis k_D , which correspond to the third and fourth standardized moments of the radar Doppler spectrum, and are respectively a measure of the degree of asymmetry and of peakedness exhibited by the spectrum (for a Gaussian curve, these measurements take a value of 0 and 3 respectively). The assumptions involved are the presence of cloud and drizzle particles in the radar sampling volume and the use of truncated lognormal PSDs to describe the cloud and drizzle

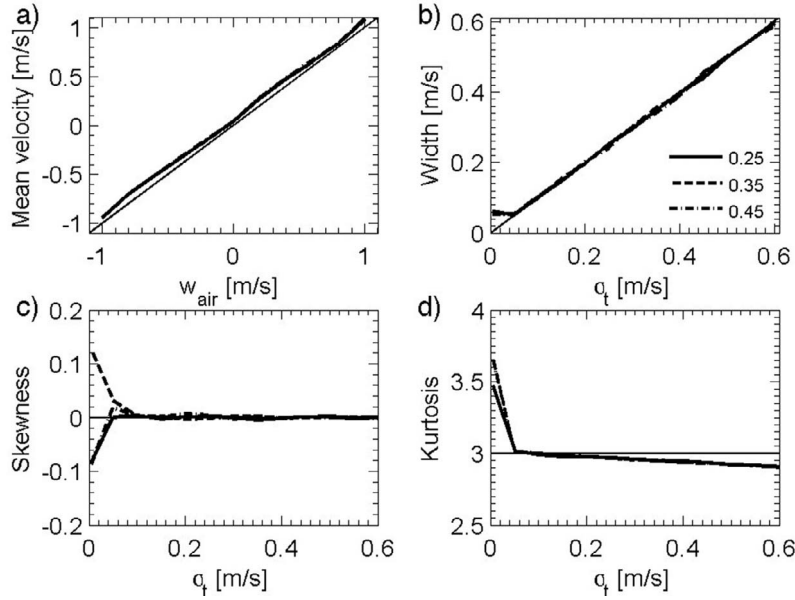


Figure 2. (a) Mean Doppler velocity of simulated radar Doppler spectra from a cloud PSD with median radius $r_{o,c} = 6.5 \mu\text{m}$ and three different values of logarithmic width $\sigma_{x,c} = (0.25, 0.35, \text{ and } 0.45)$ as a function of the simulated vertical air motion w_{air} , (b) spectrum width of simulated radar Doppler spectra for the same input cloud PSD as a function of the input turbulence broadening parameter σ_t , (c) skewness of simulated radar Doppler spectra for the same input cloud PSD as a function of the input turbulence broadening parameter σ_t , and (d) kurtosis of simulated radar Doppler spectra for the same input cloud PSD as a function of the input turbulence broadening parameter σ_t .

size distributions. The k th moment of a truncated lognormal distribution is

$$\langle r^k \rangle = \frac{r_o^k}{2} \exp\left(\frac{k^2 \sigma_x^2}{2}\right) F(k), \quad (7a)$$

$$F(k) = \text{erf}\left(\frac{\ln(r_{max}/r_o) - k\sigma_x}{\sqrt{2}\sigma_x}\right) - \text{erf}\left(\frac{\ln(r_{min}/r_o) - k\sigma_x}{\sqrt{2}\sigma_x}\right), \quad (7b)$$

where r_{min} and r_{max} are respectively the lower and upper bounds of the distribution and erf is the error function. The function $F(k)/2$ accounts for the use of a truncated PSD [Feingold and Levin, 1986] and its omission results in the expression discussed by Frisch *et al.* [1995]. For a cloud PSD, the lower bound typically doesn't affect the moments, and the second erf in the function $F(k)$ takes the value of -1 .

[15] Cloud and drizzle particles have typical sizes that allow the use of the Rayleigh approximation to describe the scattering of the radar's millimeter wavelength electromagnetic radiation. Thus, a full mathematical formulation of the five considered parameters is possible if the cloud and drizzle PSDs have a known shape and size-velocity relationship. The k th velocity moment of the radar Doppler spectrum of drizzle is given by:

$$\langle V^k \rangle_D = \frac{\langle r^6 [V_f(r)]^k \rangle}{\langle r^6 \rangle}, \quad (8)$$

where $V_f(r)$ is the fall velocity of the particle with radius r [Frisch *et al.*, 1995]. Using the aforementioned general expressions, the observed radar Doppler spectrum parameters are considered for two general cases: a radar sampling volume containing only cloud particles and a radar sampling volume containing both cloud and drizzle particles. The cases where drizzle dominates the radar Doppler moments or only drizzle particles are present in the radar sampling volume (i.e., below the cloud base) are special cases of the latter classification.

3.1. Radar Sampling Volume Contains Only Cloud Droplets

[16] If only cloud droplets are present in the radar sampling volume, the microphysical information that can be retrieved is limited. The radar reflectivity can be linked to the cloud PSD parameters, especially if integrated liquid water path measurements are available, but linkages are not available for the other radar moments [e.g., Frisch *et al.*, 1998, 2002]. Turbulence (w_{air} and ε) dominates the location (mean Doppler velocity) and the shape (spectrum width) of the radar Doppler spectrum (Figure 2). This is attributable to the negligible fall velocity of the cloud droplets and their very narrow range of fall velocities. As a result, the vertical component of air motion (w_{air}) determines the observed mean Doppler velocity and the turbulence broadening parameter (σ_t) determines the observed spectrum width. Thus, traditionally, the Doppler velocity of cloud spectral peak is used to retrieve the vertical air motion (w_{air}), and the spectrum width of the cloud spectral peak is used to retrieve the eddy dissipation rate (ε) with relatively small uncertainties [Kollias *et al.*, 2001; O'Connor

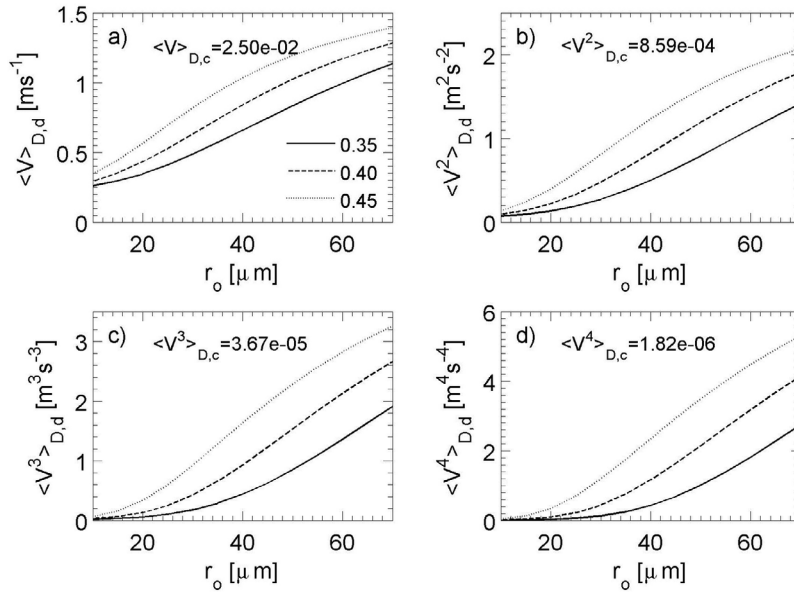


Figure 3. The first four velocity moments for a drizzle PSD as a function of drizzle median radius $r_{o,d}$ and for three different PSD logarithmic widths $\sigma_{x,d}$ (0.35, 0.40, and 0.45). The corresponding velocity moment for a cloud PSD with $r_{o,c} = 6.5 \mu\text{m}$ and logarithmic width $\sigma_{x,c} = 0.35$ is shown in the legend.

et al., 2005; Kollias and Albrecht, 2010]. If turbulence broadening determines the shape of the radar Doppler spectrum, the Doppler spectrum skewness should be around zero and kurtosis near 3. Simulations of radar Doppler spectra for a typical cloud PSD for a variety of dynamical conditions (w_{air} and σ_l) agree with the assertion that dynamics control all but the radar reflectivity measurement of a cloud PSD (Figure 2).

3.2. Radar Sampling Volume Contains Both Cloud and Drizzle Droplets

[17] The zeroth moment of the radar Doppler spectrum (i.e., the radar reflectivity factor) for an individual PSD or the combined PSD can be expressed as:

$$Z_i = 2^6 N_{i,r}^6 e^{18\sigma_{x,i}^2} F_i(6)/2, \quad (9a)$$

$$Z_{\text{meas}} = Z_c + Z_d = Z_d(1 + \chi), \quad (9b)$$

where the subscript i indicates either cloud (c) or drizzle (d) PSD. The parameter $\chi = Z_c/Z_d$ is used here to determine the relative contribution of the cloud and drizzle PSDs to the observed radar Doppler spectrum parameters. The expression for the measured radar reflectivity factor is straightforward since turbulence does not influence the measurement. The parameter χ can be expressed also as a function of the ratio of cloud liquid water content to the drizzle liquid water content and other parameters of the cloud and drizzle PSDs:

$$\chi = \frac{N_d}{N_c} \left(\frac{LWC_c}{LWC_d} \right)^2 \exp \left[9 \left(\sigma_{x,c}^2 - \sigma_{x,d}^2 \right) \right] \frac{F_c(6)}{F_c(3)^2} \frac{F_d(3)^2}{F_d(6)}. \quad (10)$$

[18] Despite the explicit dependences of the factor χ on the cloud PSD parameters (both written above and hidden in

the functions $F_c(k)$), those dependences are rather weak for typical values of stratocumulus clouds. For instance, the dependence on $r_{o,c}$ comes only from the ratio $F_c(6)/F_c(3)^2$, which is minor for the range of values reported by Miles *et al.* [2000].

[19] For the combination of two nonoverlapping truncated lognormal distributions, the k th velocity moment is a weighted average of the k th velocity moment of each distribution, as follows:

$$\langle V^k \rangle_D = \frac{Z_c \langle V^k \rangle_{D,c} + Z_d \langle V^k \rangle_{D,d}}{Z_c + Z_d} \approx \frac{\langle V^k \rangle_{D,d}}{1 + \chi}. \quad (11)$$

[20] The suggested approximation is based on the fact that the cloud PSD velocity moments $\langle V^k \rangle_{D,c}$ are negligible compared to their corresponding drizzle velocity moments (Figure 3). Using the last equation and the formal definition of each moment, we obtain the following formulas for the variance (σ_{PSD}^2), skewness (s_{PSD}) and kurtosis (k_{PSD}) of an ideal quiet air ($w_{\text{air}} = 0$, $\varepsilon = 0$) radar Doppler spectrum of combined truncated cloud and drizzle PSDs:

$$\begin{aligned} \sigma_{PSD}^2 &= \langle V^2 \rangle_D - \langle V \rangle_D^2 \\ &\approx \frac{\sigma_d^2 + \chi \langle V^2 \rangle_{D,d}}{[1 + \chi]^2}, \end{aligned} \quad (12a)$$

$$\begin{aligned} s_{PSD} &= \frac{\langle V^3 \rangle_D - 3\langle V \rangle_D \langle V^2 \rangle_D + 2\langle V \rangle_D^3}{\sigma_{PSD}^3} \\ &\approx \frac{\sigma_d^3 s_d + \chi \left[\langle V^3 \rangle_{D,d} (2 + \chi) - 3\langle V \rangle_{D,d} \langle V^2 \rangle_{D,d} \right]}{\left[\sigma_d^2 + \chi \langle V^2 \rangle_{D,d} \right]^{3/2}}, \end{aligned} \quad (12b)$$

$$k_{PSD} = \frac{\langle V^4 \rangle_D - 4\langle V \rangle_D \langle V^3 \rangle_D + 6\langle V \rangle_D^2 \langle V^2 \rangle_D - 3\langle V \rangle_D^4}{\sigma_{PSD}^4}$$

$$\approx \frac{\sigma_d^4 k_d + \chi \left[\langle V^4 \rangle_{D,d} (3 + 3\chi + \chi^2) - 4\langle V \rangle_{D,d} \langle V^3 \rangle_{D,d} (2 + \chi) + 6\langle V \rangle_{D,d}^2 \langle V^2 \rangle_{D,d} \right]}{\left[\sigma_d^2 + \chi \langle V^2 \rangle_{D,d} \right]^2}. \quad (12c)$$

[21] Thus, the quiet air radar Doppler spectrum variance (σ_{PSD}^2), skewness (s_{PSD}) and kurtosis (k_{PSD}) can be expressed as a function of the parameter χ , the drizzle-only quiet air radar Doppler spectrum velocity moments (first corresponding to the mean Doppler velocity $\langle V \rangle_{D,d}$, second $\langle V^2 \rangle_{D,d}$, third $\langle V^3 \rangle_{D,d}$, and fourth $\langle V^4 \rangle_{D,d}$) and parameters of interest (variance σ_d^2 , skewness s_d , and kurtosis k_d). The four drizzle-only Doppler spectrum velocity moments can be expressed as a function of the assumed truncated lognormal PSD parameters and the drizzle fall velocity relationship (Appendix A).

3.3. Effect of Turbulence on the Radar Doppler Spectra Moments

[22] The final step is to account for the effect of turbulence on the observed and modeled radar Doppler spectra. The effect of w_{air} is a shift of the radar Doppler spectrum and impacts only the observed mean Doppler velocity:

$$\langle V \rangle_{D,meas} = \langle V \rangle_D + w_{air}. \quad (13)$$

[23] The impact of the turbulent eddies with spatial scales smaller than the radar sampling volume is formulated using a convolution of the turbulence PDF with the quiet air radar Doppler spectrum. The resulting n th centered moment after the convolution can be expressed using the formula provided by *Laury-Micoulaud* [1976]:

$$\langle x^n \rangle_{psd*turb} = \sum_{i=0}^n \frac{n!}{(i)!(n-i)!} \langle x^i \rangle_{psd} \langle x^{n-i} \rangle_{turb} \quad (14)$$

where $\langle x^n \rangle_{psd*turb}$ is the n th centered moment of the convolution of the PSD and turbulence functions. Since the turbulence function is a Gaussian with a mean value of zero and known 2nd centered moment (σ_t^2), the resulting spectrum is characterized by the following convolved moments:

$$\sigma_{meas}^2 = \sigma_{PSD}^2 + \sigma_t^2, \quad (15a)$$

$$s_{meas} = \frac{\sigma_{PSD}^3 s_{PSD}}{(\sigma_{PSD}^2 + \sigma_t^2)^{3/2}}, \quad (15b)$$

$$k_{meas} = \frac{\sigma_{PSD}^4 k_{PSD} + 3\sigma_t^2 (\sigma_t^2 + 2\sigma_{PSD}^2)}{(\sigma_{PSD}^2 + \sigma_t^2)^2}. \quad (15c)$$

[24] The above relationships (13), (15a), (15b), and (15c) relate the mean Doppler velocity, spectrum width, skewness

and kurtosis of the cloud radar Doppler spectrum to the microphysical and dynamical conditions. For clarity, the expressions for the drizzle-only PSD radar Doppler spectrum velocity moments (first corresponding to the mean Doppler velocity $\langle V \rangle_{D,d}$, second $\langle V^2 \rangle_{D,d}$, third $\langle V^3 \rangle_{D,d}$, and fourth $\langle V^4 \rangle_{D,d}$) and parameters of interest (variance σ_d^2 , skewness s_d , and kurtosis k_d) are presented in Appendix A.

[25] The parameter $\chi = Z_c/Z_d$ plays a critical role in the determination of the radar Doppler spectra moments. Changes in mean Doppler velocity, spectrum width, skewness and kurtosis of simulated radar Doppler spectra for a combination of cloud and drizzle PSD as a function of the parameter χ is shown in Figure 4. The parameter χ changes by increasing the drizzle PSD median radius $r_{o,d}$ for three different logarithmic widths $\sigma_{x,d} = (0.35, 0.40 \text{ and } 0.45)$ while the cloud PSD parameters are held constant ($N_c = 75 \text{ cm}^{-3}$, $r_{o,c} = 6.5 \mu\text{m}$ and logarithmic width $\sigma_{x,c} = 0.35$). At large χ values, cloud contributions to the radar Doppler spectra moments dominate. Thus, the simulations show near zero mean Doppler velocity (no vertical air motion), spectrum width value that equals the simulated turbulence broadening (0.2 ms^{-1} , fixed for the simulations), near zero skewness and kurtosis of around 3. This is consistent with the results shown in Figure 2. As χ decreases, the relative contribution of the drizzle PSD to the radar Doppler spectra moments increases.

[26] The radar Doppler moment that is least sensitive to the increasing drizzle radar reflectivity is the mean Doppler velocity. Drizzle starts influencing mean Doppler velocity estimates for values of $\log(\chi)$ close to zero (i.e., the cloud radar reflectivity Z_c is close to the drizzle radar reflectivity Z_d). The spectrum width increase due to the wider range of particle fall velocities starts earlier (for higher χ values). At even lower χ values the spectrum width reaches a maximum and then decreases. This is caused by the artificial increase in drizzle reflectivity factor resulting from an increase in the mean radius.

[27] Skewness and kurtosis exhibit even higher sensitivity to small amounts of drizzle. The positive skewness is the result of a dominant cloud peak and a weaker drizzle bump at more positive Doppler velocities (fall velocities). As the drizzle contribution increases, the skewness decreases and even acquires negative values due to the dominance of the drizzle peak and a weak cloud bump at less positive Doppler velocities. Finally, the Doppler spectra kurtosis initially increases due to the presence of a wider tail (weak drizzle bump) and then decreases as the drizzle spectral peak increases and dominates the shape of the Doppler spectrum. The simulated trends in the radar Doppler moments as a function of the drizzle strength can only be used as a guiding tool since

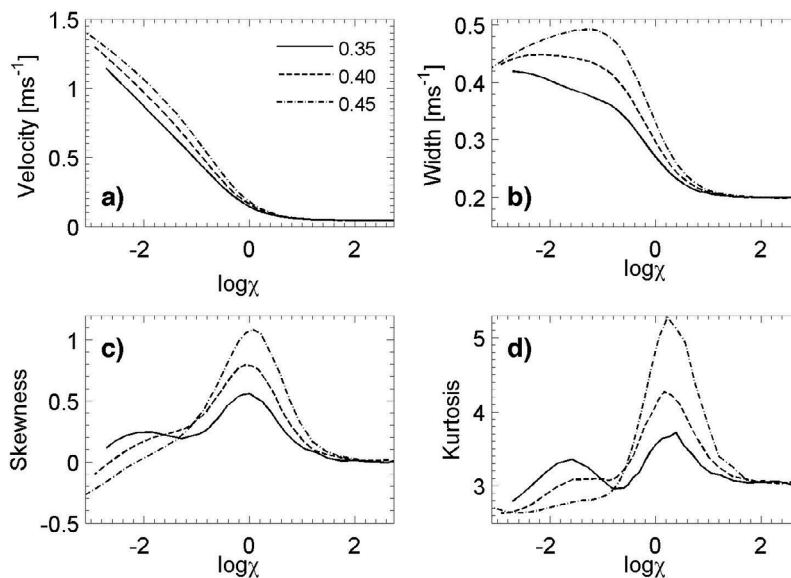


Figure 4. (a) Mean Doppler velocity, (b) spectrum width, (c) skewness, and (d) kurtosis of simulated radar Doppler spectra for a combined cloud and drizzle PSD as a function of parameter χ . The cloud PSD parameters are constant ($N_c = 75 \text{ cm}^{-3}$, $r_{o,c} = 6.5 \text{ }\mu\text{m}$ and logarithmic width $\sigma_{x,c} = 0.35$), while the parameter χ changes by increasing the drizzle PSD parameter $r_{o,d}$ for three different logarithmic widths $\sigma_{x,d} = (0.35, 0.40, \text{ and } 0.45)$.

the drizzle contribution in the simulation increases in an artificial way.

3.4. Effect of SNR and Doppler Spectra Velocity Resolution on the Radar Doppler Spectra Moments

[28] The signal-to-noise ratio (SNR) and the Doppler velocity resolution are two parameters often used to describe the quality of a radar Doppler spectrum. Low SNR conditions can have a great impact in the uncertainty associated with the moment estimates. Furthermore, low Doppler velocity resolution can greatly affect the accuracy of the moment estimates, especially for narrow spectra. Simulations over a wide range of SNR conditions and for different Doppler spectra velocity resolutions were performed to assess the noisiness of the skewness and kurtosis estimates (Figure 5). A drizzle-only PSD with fixed logarithmic width ($\sigma_x = 0.40$ and variable median radius (r_o : $10\text{--}70 \text{ }\mu\text{m}$) is used. The turbulence broadening term is fixed ($\sigma_t = 0.2 \text{ ms}^{-1}$) in all simulations. For comparison, the theoretical skewness and kurtosis values of the simulated Doppler spectra using the equations in Appendix A are shown in Figure 5 (thick gray lines). SNR conditions equal to or higher than 0 dB are needed in order to get a low-uncertainty estimates of the moments. Similarly, Doppler velocity resolution better than 10 cm s^{-1} is required also. The latter is achieved for both cloud radar systems used in this study (section 2), while the former criterion is typically fulfilled when drizzle is present above the cloud base, which is the area of main interest here.

[29] The overall agreement of the predicted (analytically) and measured (simulated) values of skewness and kurtosis is encouraging and suggests that the analytical expressions (section 3.3) are capable of predicting the Doppler moments for a variety of microphysical and dynamical conditions. Extensive testing (not shown here) of the validity of the

presented formulas against the simulator output has been performed with consistently good agreement.

3.5. Observations of Radar Doppler Spectra Skewness and Kurtosis

[30] The deviation of radar Doppler spectra shape from normal distribution characteristics is a good indicator of microphysical information content, as captured in shape parameters (e.g., skewness and kurtosis). Extensive observations from continental (SGP) and maritime (Graciosa island) ARM sites were used to study the Doppler spectra morphology. Composites of radar Doppler spectra for certain values of skewness and kurtosis can be constructed using constraints on their radar reflectivity and total width. The total width is defined as the Doppler velocity span (ms^{-1}) from the left to the right edge of the Doppler spectrum. Typical examples of such composites are shown in Figure 6, for a radar reflectivity of -30 dBZ and spectrum width of 0.4 ms^{-1} . In each panel, two different Doppler spectra averages as presented (solid and dashed lines) and should not be misinterpreted as derived from the same radar Doppler spectra. All observations are above the cloud base; thus, a cloud PSD is present. It is apparent that radar Doppler spectra, even at such low radar reflectivity (often used as a safe limit for drizzle-free observations) exhibit very large variability in shape. Skewness is a powerful variable for understanding the relative contribution of cloud and drizzle PSDs. Positive skewness values are associated with a dominant cloud peak at low fall velocities and weak drizzle returns at higher fall velocities (i.e., $\chi > 1$). On the other hand, negative values are associated with a dominant drizzle peak (i.e., $\chi < 1$). Kurtosis is more related to the peakedness of a Doppler spectrum. Values of kurtosis below 3 indicate a platykurtic (kurtosis less than 3) distribution of spectral power around the mean. Such

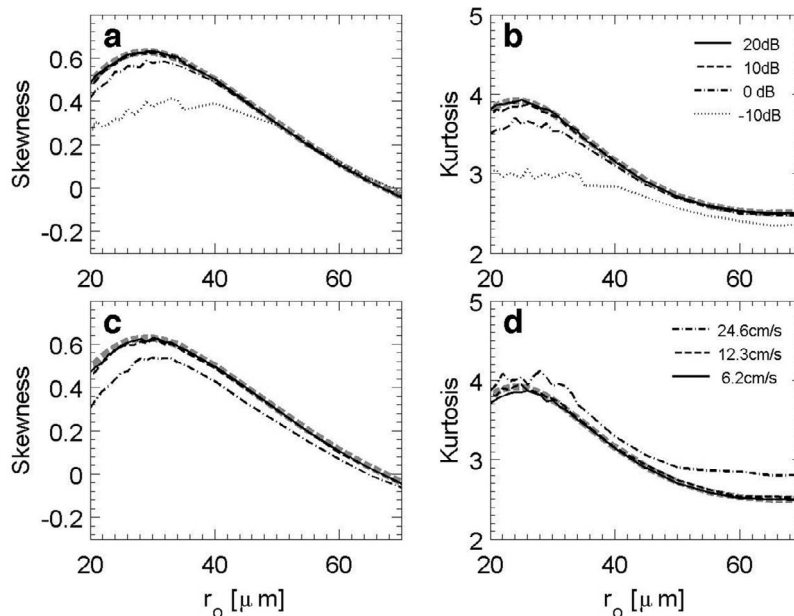


Figure 5. Effect (a, b) of the radar Doppler spectrum signal-to-noise ratio (SNR) (velocity resolution of 6.2 cm s^{-1}) and (c, d) of the Doppler spectrum velocity resolution (SNR of 10 dB) on the skewness (Figures 5a and 5c) and kurtosis (Figures 5b and 5d) estimates of simulated radar Doppler spectra. The thick, gray dashed line represents the theoretical value estimated using the expressions for skewness and kurtosis provided in the text. The various thick lines are the estimated values of skewness and kurtosis obtained from the postprocessing of simulated radar Doppler spectra generated with the same input parameters.

Doppler spectra can occur when cloud and drizzle distributions are of similar strength (dashed-line spectra with kurtosis values K : 2.00–2.43 in Figure 6). High values of kurtosis indicate a leptokurtic (kurtosis more than 3) distribution, which can be due to the presence of a narrow PSD or the presence of weak spectral bumps (e.g., early drizzle growth).

4. Applications to Radar-Based Drizzle Retrievals

[31] The introduction of the radar Doppler spectrum skewness and kurtosis as additional radar observable parameters can lead to enhancement in our ability to detect the onset of precipitation (e.g., drizzle particle generation) and constraints in quantitative drizzle microphysical retrievals.

4.1. Detection of Early Drizzle Onset in Liquid Clouds

[32] Knowledge of the presence of drizzle particles in liquid stratiform clouds is of paramount importance. Identifying the location in clouds where drizzle initiation is generated through the autoconversion process is important for understanding precipitation onset in shallow clouds. In addition, different algorithms are needed for nonprecipitating and drizzling clouds; for example, drizzle limits the applicability of single-radar techniques to retrieve the LWC. In profiling cloud radar observations of marine stratus, the presence of drizzle size particles is usually inferred by the presence of radar echoes below the visible cloud base or by using an empirical radar reflectivity threshold Z_{th} . *Sauvageot and Omar* [1987] suggested a Z_{th} of -15 dBZ for coastal cumulus and stratocumulus. *Frisch et al.* [1995] proposed a value between -17 and -15 dBZ to detect the presence of enough drizzle in the sampling volume of marine stratocumulus to affect the radar

measurements. *Mace and Sassen* [2000] proposed a lower value (-20 dBZ) for continental liquid clouds. *Baedi et al.* [2002] used a jump of approximately 10 dB in reflectivity between drizzle-free and drizzling clouds. They suggested for marine, coastal and continental clouds a Z_{max} of -20 dBZ for no drizzle and a Z_{min} of -10 dBZ for drizzling clouds. *Wang and Geerts* [2003] used values from -19 to -16 dBZ for marine clouds and proposed a Z_{th} profile as an increasing function of normalized height within cloud, defined only in the lower half of the cloud. *Krasnov and Russchenberg* [2005] provided different Z_{th} between drizzle-free and light drizzle and between light and heavy drizzle clouds. Finally, in a recent study, *Liu et al.* [2008] proposed a parameterization of the radar reflectivity threshold Z_{th} for the transition from cloud to cloud mixed with drizzle as a function of the total cloud droplet concentration. Another suggested approach is to use the vertical structure of the radar reflectivity profile in liquid clouds to discriminate between drizzling and drizzle-free areas in clouds [*Fox and Illingworth*, 1997; *Mace and Sassen*, 2000]. In particular, small radar reflectivity Z values that steadily increase with altitude is a good indicator of drizzle free conditions [*Wang and Geerts*, 2003].

[33] It is apparent that past studies focused on identifying a radar reflectivity threshold value beyond which drizzle particles dominate the radar observables. However, the initial generation and growth of drizzle particles and their subsequent impact on the radar observables occur at a much lower radar reflectivity threshold. Identifying the location where drizzle onset occurs in liquid clouds can improve our understanding of spectral broadening in warm clouds. To accomplish this, we propose the use of the radar Doppler spectrum skewness as

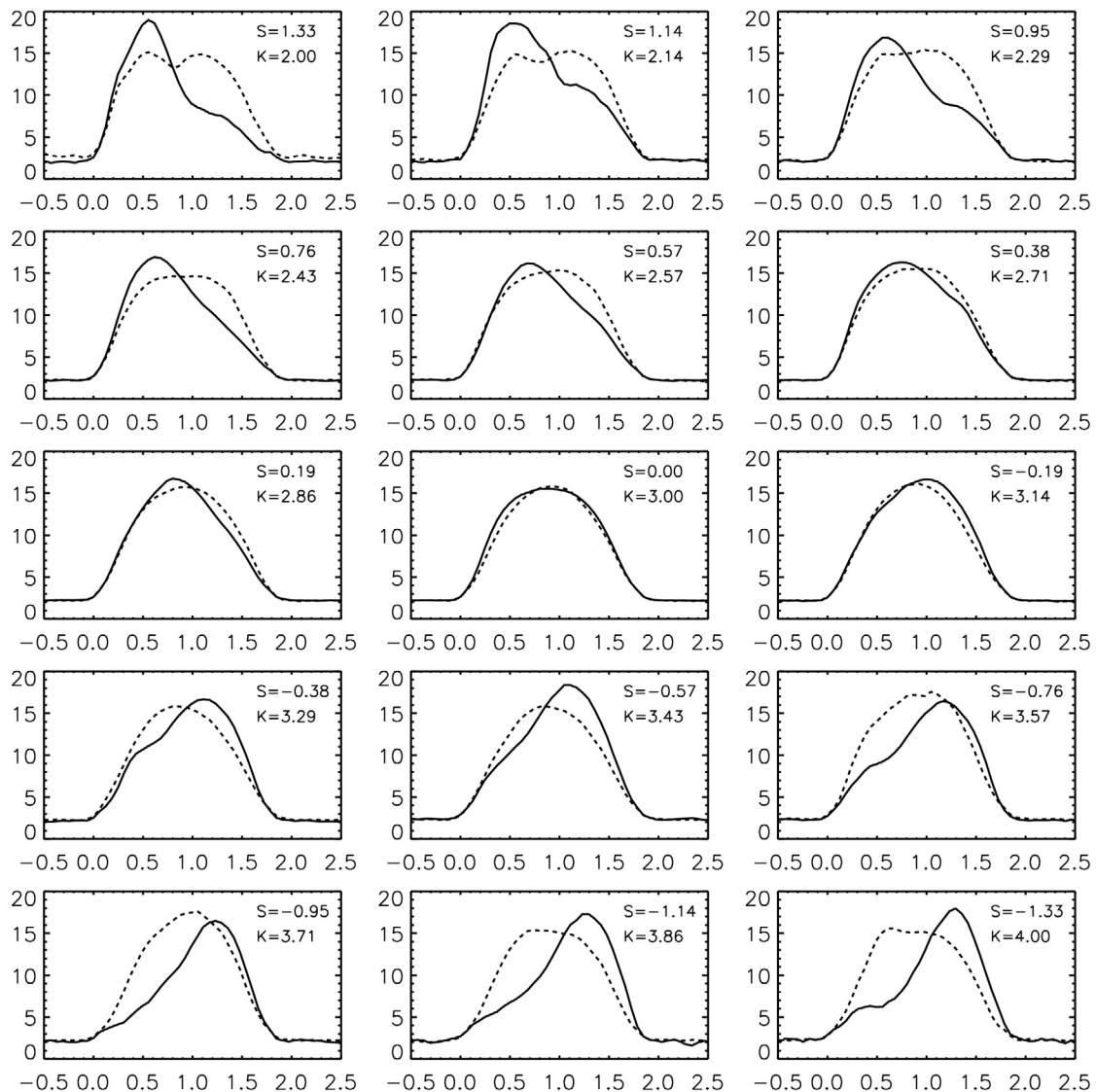


Figure 6. Examples of observed W band radar Doppler spectra for a wide range of skewness and kurtosis values at the ARM AMF Graciosa site. In each panel, two different Doppler spectra averages are presented (solid and dashed lines) and should not be misinterpreted as derived from the same radar Doppler spectra. The solid lines correspond to Doppler spectra composites (averages) constructed using Doppler spectra with a radar reflectivity around -30 dBZ, spectrum width around 0.4 ms^{-1} , and skewness values near the reported S value in each panel. The dashed lines correspond to Doppler spectra composites (averages) constructed using Doppler spectra with a radar reflectivity around -30 dBZ, spectrum width around 0.4 ms^{-1} , and kurtosis values near the reported K value in each panel.

a very sensitive parameter for the detection of drizzle onset. First, we will demonstrate that cloud-only radar Doppler spectra can be approximated as Gaussian and thus have near-zero skewness. This will be shown using both observations and Doppler spectra simulations. Assuming a cloud-only PSD, the observed radar Doppler spectrum is simulated and its skewness for a wide range of logarithmic width values and median radii is investigated (Figure 7). The simulations demonstrate that the mean skewness of cloud-only PSD is zero for all conditions. More importantly, the standard deviation of the simulated skewness is below 0.1 for median radius values higher than 6 μm , independent of the assumed

PSD logarithmic width and for typical turbulence broadening values (0.2 – 0.3 ms^{-1}). At low median radii (below 5 – 6 μm) the estimated standard deviation is higher and this can be attributable to the impact of the PSD shape at low median radius values. Turbulence broadening is largely responsible for the near-zero skewness radar Doppler spectra (Figure 7).

[34] One full day of cloud radar observations from the AMF/Graciosa field deployment are used to demonstrate the transition of skewness as a function of radar reflectivity (Figure 8). The cloud radar observations above the cloud base are partitioned in narrow radar reflectivity bins (2 dBZ wide) and the bin average radar Doppler spectra skewness

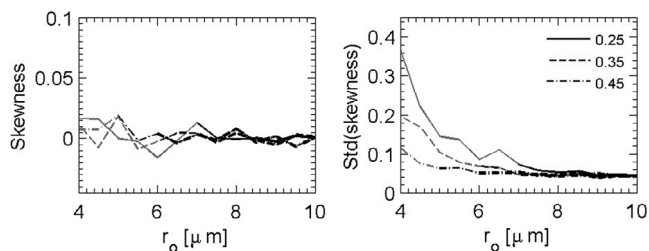


Figure 7. Simulations of cloud-only radar Doppler spectra skewness using the forward model. (left) The mean skewness and (right) the standard deviation of the simulated skewness. Three different logarithmic width values are used [σ_x : 0.25, 0.35, and 0.45], and the median radius r_o varies from 4 to 10 μm . One hundred simulated radar Doppler spectra were used at each median radius and logarithmic width combination to estimate the mean and standard deviation of the radar Doppler spectra skewness.

and Doppler velocity are shown (Figure 8). At very low reflectivity, the skewness is near zero. As drizzle develops at higher (positive) fall velocities, a positive tail develops in the observed radar Doppler spectra, leading to a positive increase of the average radar Doppler spectrum skewness. This occurs at radar reflectivity values as low as -40 dBZ where the cloud contribution to the observed radar reflectivity is still dominant. At higher reflectivities, the skewness reaches a positive plateau and starts to decrease as the drizzle spectral peaks grow relative to the cloud peak. At higher radar reflectivity values, skewness crosses zero and becomes negative due to the fact that the drizzle peak is dominant and the cloud peak on its left (lower velocity) side of the Doppler spectrum creates a negative skewness. Noticeably, the mean Doppler velocity evolution as a function of the radar reflectivity exhibits transition points that match very well the different skewness regimes.

4.2. Improved Quantitative Drizzle PSD Retrievals

[35] Previous methods of retrieving cloud and drizzle properties using radar observations have focused on two regimes: cloud PSD only ($\chi \rightarrow \infty$) radar observations and drizzle PSD only ($\chi \rightarrow 0$) radar observations (see Table 2). At these limits all observed radar Doppler spectrum parameters are determined by the cloud and drizzle PSD respectively. As it has been discussed, in the cloud-only regime, only the radar reflectivity is directly related to the cloud PSD parameters and all other parameters are related to cloud dynamics (w_{air} and ε). Contrarily, in the drizzle-only regime, both dynamics and microphysics (w_{air} , ε , N_d , $r_{o,d}$, $\sigma_{x,d}$) contribute to the observed radar Doppler spectrum parameters. Between these two extremes (often differentiated using a radar reflectivity threshold) lies a transition regime from cloud only PSD to cloud and drizzle PSD where the cloud PSD still contributes to the radar observations. This regime is of great interest due to the cloud to drizzle transition. Here, detailed analytical expressions that relate all five radar parameters to cloud and drizzle PSD parameters and dynamics were presented. These relationships offer a seamless transition of the parameters across all three regimes and can be used to constrain retrievals of drizzle PSD parameters if the

assumptions related to the proposed radar Doppler spectra model are valid. In the mixed cloud and drizzle regime, both the cloud PSD and drizzle PSD contribute to the observed radar Doppler spectrum. As a result, this is the regime where skewness and kurtosis exhibit their greatest changes and can be used to constrain the retrievals. For example, the mixed cloud and drizzle regime includes skewness values that start deviating from near zero to negative (when drizzle dominates the radar Doppler spectrum). It is interesting to note that in this regime, the cloud spectral peak is dominant (e.g., $\chi > 1$) or at least not fully masked by the drizzle peak ($\chi > 0.01$). As a result, this is a regime for which a full radar Doppler spectrum-based retrieval technique could be developed to

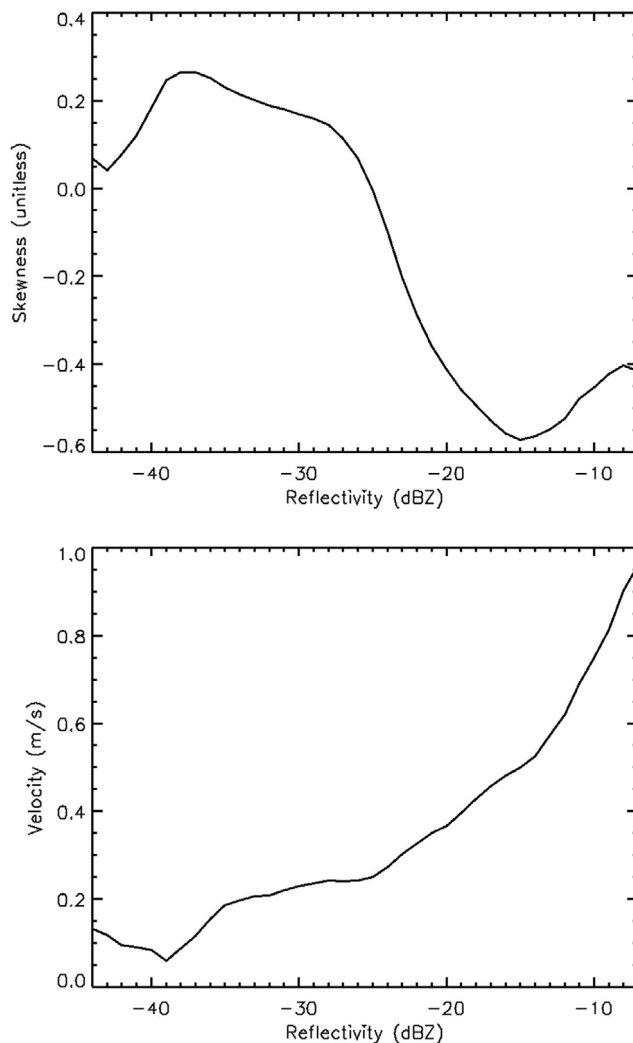


Figure 8. Relationship between (top) observed radar Doppler spectra skewness and (bottom) mean Doppler velocity as a function of observed radar reflectivity. The observations are from the AMF deployment in the Azores and represent 24 h of a stratus layer with drizzle. Reflectivity bins of 2 dBZ were used to construct the mean values of skewness and Doppler velocity as a function of the radar reflectivity. The lines correspond to the mean value of skewness and Doppler velocity within the 2 dBZ bins.

Table 2. Relationship Between Millimeter-Wave Radar Doppler Spectra Moments and Stratocumulus Dynamics and Microphysics

Radar Doppler Spectrum Parameters	Cloud Only ($\chi \rightarrow \infty$)	Cloud and Drizzle ($100 > \chi > 0.01$)	Drizzle Only ($\chi \rightarrow 0$)
Z (Reflectivity)	$f(N_c, r_{o,c}, \sigma_{x,c})$	$(1 + \chi) \cdot f(N_d, r_{o,d}, \sigma_{x,d})$	$f(N_d, r_{o,d}, \sigma_{x,d})$
V_D (Mean Doppler velocity)	w_{air}	$w_{\text{air}} + f(r_{o,d}, \sigma_{x,d})/(1 + \chi)$	$w_{\text{air}} + f(r_{o,d}, \sigma_{x,d})$
σ_D (Spectrum Width)	$f(\varepsilon)$	$f(\varepsilon) + f(\chi, r_{o,d}, \sigma_{x,d})$	$f(\varepsilon) + f(r_{o,d}, \sigma_{x,d})$
s_D (Skewness)	$f(\varepsilon, r_{o,c}, \sigma_{x,c}) \approx f(\varepsilon)$	$f(\varepsilon, \chi, r_{o,d}, \sigma_{x,d})$	$f(\varepsilon, r_{o,d}, \sigma_{x,d})$
k_D (Kurtosis)	$f(\varepsilon, r_{o,c}, \sigma_{x,c}) \approx f(\varepsilon)$	$f(\varepsilon, \chi, r_{o,d}, \sigma_{x,d})$	$f(\varepsilon, r_{o,d}, \sigma_{x,d})$

identify the cloud spectral peak and use it to retrieve the dynamical parameters (w_{air} and ε). In the drizzle only regime ($\chi \rightarrow 0$), the drizzle PSD spectral peak often masks the cloud spectral peak, making the retrieval of the dynamical parameters increasingly challenging. However, skewness and kurtosis measurements are affected by the drizzle PSD parameters ($r_{o,d}$ and $\sigma_{x,d}$) and can be used to constrain the retrievals of drizzle PSD parameters in the drizzle only regime. For instance, the skewness, kurtosis and spectrum width of the radar Doppler spectrum can be expressed as function of the eddy dissipation rate ε , drizzle median radius $r_{o,d}$ and drizzle PSD logarithm width $\sigma_{x,d}$. This can lead to the retrieval of the drizzle PSD shape ($r_{o,d}$, $\sigma_{x,d}$) without knowledge of the vertical air motion. The radar reflectivity can then be used to derive the drizzle PSD total number concentration. Thus, the 5-parameter approach extends the *Frisch et al.* [1995] approach that linked radar observations with drizzle PSD parameters without suggesting a method for decomposing the dynamical and microphysical contributions to the radar observables.

5. Summary

[36] This paper is part one of a study that introduces a new, comprehensive approach for using radar Doppler spectra observations in liquid clouds that contain drizzle droplets. This study argues that cloud radar Doppler spectra are usually highly asymmetrical (non-Gaussian) and thus contain information about the cloud microphysics and dynamics. In addition to the usual three moments of the radar Doppler spectrum (reflectivity, mean Doppler velocity and spectral width) two parameters (the skewness and kurtosis of the radar Doppler spectrum) are introduced to describe its shape. The link between cloud/drizzle microphysics and dynamics and radar observables is accomplished with two complementary methods. First, a detailed radar Doppler spectrum forward model is presented. The forward model is tuned for the ARM cloud radar characteristics and its input are detailed cloud and drizzle PSDs, information about vertical air motion, and eddy dissipation rate within the radar sampling volume. The forward model allows the microphysical model output to be linked with radar observations. In addition, analytical relationships that link all five radar Doppler spectra parameters to cloud microphysics and dynamics are presented. The analytical relationships are used to explore the behavior of the five radar Doppler spectra parameters for a variety of dynamical and microphysical conditions and especially their behavior during drizzle onset and subsequent growth. The generality of the proposed relationships between cloud microphysics and dynamics and radar observables was validated using radar Doppler spectra simulations.

[37] It was established that the radar Doppler spectra for a cloud-only PSD is well approximated by a Gaussian. Fur-

thermore, it was established that the skewness of the radar Doppler spectra is very sensitive to the development of a weak spectral bump at the higher fall velocity side of the radar Doppler spectrum. Such small spectral bumps result from the autoconversion process that leads to drizzle onset in warm clouds. Thus, skewness is recommended as a more sensitive indicator of early drizzle onset rather than radar reflectivity or Doppler velocity, which are sensitive only when the drizzle contribution to the total observed reflectivity is significantly larger than the cloud contribution. The possible utility of radar Doppler spectrum skewness and kurtosis as additional constraints for the retrieval of drizzling cloud microphysics and dynamics has been demonstrated. Adjoining retrievals could be used to further constrain the algorithm (e.g., lidar below the cloud base and microwave radiometer in cloud-only profiles). The measurements will provide detailed information of the vertical organization of the dynamical and microphysical fields in stratus clouds.

Appendix A: Radar Doppler Spectra Moments for a Drizzle-Only Truncated Lognormal PSD

[38] Appendix A presents the derivation of analytical expressions for the radar Doppler spectra moments for a drizzle-only PSD. The assumptions involved are: the absence of turbulence and the use of a truncated lognormal function described by the parameters (N_d , $r_{o,d}$, $\sigma_{x,d}$, r_{max} and r_{min}) to describe the drizzle PSD. The k th moment of a truncated lognormal distribution is obtained from (7a) with (7b) applied to drizzle

$$\langle r^k \rangle_d = \frac{r_{o,d}^k}{2} \exp\left(\frac{k^2 \sigma_{x,d}^2}{2}\right) F_d(k)$$

$$F(k) = \text{erf}\left(\frac{\ln(r_{\text{max}}/r_{o,d}) - k\sigma_{x,d}}{\sqrt{2}\sigma_{x,d}}\right) - \text{erf}\left(\frac{\ln(r_{\text{min}}/r_{o,d}) - k\sigma_{x,d}}{\sqrt{2}\sigma_{x,d}}\right),$$

where r_{min} and r_{max} are respectively the lower and upper bounds of the distribution and erf is the error function. The function $F_d(k)/2$ accounts for the use of a truncated PSD and its omission results in the expression discussed by *Frisch et al.* [1995]. The zeroth moment of the radar Doppler spectrum (i.e., the radar reflectivity factor) is independent of the particle fall velocity and for a truncated lognormal PSD can be expressed as:

$$Z_d = 2^6 N_d r_{o,d}^6 e^{18\sigma_{x,d}^2} F_d(6)/2.$$

[39] Additional moments of the radar Doppler spectrum require the definition of the k th velocity moment of the radar Doppler spectrum given in (8). Using these expressions and defining $F_d^*(k) = F_d(k)/F_d(6)$, we can express the drizzle-

only PSD radar Doppler spectrum velocity moments (first to fourth) as

$$\begin{aligned}\langle V \rangle_{D,d} &= ar_{o,d} \exp\left(13\sigma_{x,d}^2/2\right)F_d^*(7) - b, \\ \langle V^2 \rangle_{D,d} &= a^2r_{o,d}^2 \exp\left(14\sigma_{x,d}^2\right)F_d^*(8) \\ &\quad - 2abr_{o,d} \exp\left(13\sigma_{x,d}^2/2\right)F_d^*(7) + b^2, \\ \langle V^3 \rangle_{D,d} &= a^3r_{o,d}^3 \exp\left(45\sigma_{x,d}^2/2\right)F_d^*(9) \\ &\quad - 3a^2br_{o,d}^2 \exp\left(14\sigma_{x,d}^2\right)F_d^*(8) \\ &\quad + 3ab^2r_{o,d} \exp\left(13\sigma_{x,d}^2/2\right)F_d^*(7) - b^3, \\ \langle V^4 \rangle_{D,d} &= a^4r_{o,d}^4 \exp\left(32\sigma_{x,d}^2\right)F_d^*(10) \\ &\quad - 4a^3br_{o,d}^3 \exp\left(45\sigma_{x,d}^2/2\right)F_d^*(9) \\ &\quad + 6a^2b^2r_{o,d}^2 \exp\left(14\sigma_{x,d}^2\right)F_d^*(8) \\ &\quad - 4ab^3r_{o,d} \exp\left(13\sigma_{x,d}^2/2\right)F_d^*(7) + b^4,\end{aligned}$$

as well as the drizzle-only radar Doppler spectrum parameters (variance σ_d^2 , skewness s_d , and kurtosis k_d):

$$\begin{aligned}\sigma_d^2 &= a^2r_{o,d}^2 \exp\left(13\sigma_{x,d}^2\right) \left[\exp\left(\sigma_{x,d}^2\right)F_d^*(8) - F_d^*(7)^2 \right], \\ \sigma_d^3s_d &= a^3r_{o,d}^3 \exp\left(39\sigma_{x,d}^2/2\right) \left[\exp\left(3\sigma_{x,d}^2\right)F_d^*(9) \right. \\ &\quad \left. - 3 \exp\left(\sigma_{x,d}^2\right)F_d^*(8)F_d^*(7) + 2F_d^*(7)^3 \right], \\ \sigma_d^4k_d &= a^4r_{o,d}^4 \exp\left(26\sigma_{x,d}^2\right) \\ &\quad \left[\exp\left(6\sigma_{x,d}^2\right)F_d^*(10) - 4 \exp\left(3\sigma_{x,d}^2\right)F_d^*(9)F_d^*(7) \right. \\ &\quad \left. + 6 \exp\left(\sigma_{x,d}^2\right)F_d^*(8)F_d^*(7)^2 - 3F_d^*(7)^4 \right],\end{aligned}$$

where a and b are two constants in a linear relationship representative of drizzle drops fall speed from Frisch *et al.* [1995]. Including those two sets of equations into the set of equations (12a)–(12c) (section 3.2) provides more developed approximate formulas for the variance (σ_{PSD}^2), skewness (s_{PSD}) and kurtosis (k_{PSD}).

[40] **Acknowledgments.** Support for this research was funded by the Office of Biological and Environmental Research, Environmental Sciences Division of the U.S. Department of Energy as part of the Atmospheric Radiation Measurement program.

References

- Ackerman, A. S., O. B. Toon, and P. V. Hobbs (1993), Dissipation of marine stratiform clouds and collapse of the marine boundary layer due to the depletion of cloud condensation nuclei by clouds, *Science*, *262*, 226–229, doi:10.1126/science.262.5131.226.
- Ackerman, A. S., et al. (2009), Large-eddy simulations of a drizzling, stratocumulus-topped marine boundary layer, *Mon. Weather Rev.*, *137*, 1083–1110, doi:10.1175/2008MWR2582.1.
- Albrecht, B. A., D. A. Randall, and S. Nicholls (1988), Observations of marine stratocumulus clouds during FIRE, *Bull. Am. Meteorol. Soc.*, *69*, 618–626, doi:10.1175/1520-0477(1988)069<0618:OOMSCD>2.0.CO;2.
- Atlas, D., R. C. Srivastava, and R. S. Sekhon (1973), Doppler radar characteristics of precipitation at vertical incidence, *Rev. Geophys.*, *11*, 1–35, doi:10.1029/RG011i001p00001.
- Baedi, R., R. Boers, and H. Russenberger (2002), Detection of boundary layer water clouds by spaceborne cloud radar, *J. Atmos. Oceanic Technol.*, *19*, 1915–1927, doi:10.1175/1520-0426(2002)019<1915:DOBLWC>2.0.CO;2.

- Battan, L. J. (1964), Some observations of vertical velocities and precipitation sizes in a thunderstorm, *J. Appl. Meteorol.*, *3*, 415–420, doi:10.1175/1520-0450(1964)003<0415:SOOVVA>2.0.CO;2.
- Bony, S., and J.-L. Dufresne (2005), Marine boundary layer clouds at the heart of tropical cloud feedback uncertainties in climate models, *Geophys. Res. Lett.*, *32*, L20806, doi:10.1029/2005GL023851.
- Caton, P. G. F. (1966), A study of raindrop-size distributions in the free atmosphere, *Q. J. R. Meteorol. Soc.*, *92*, 15–30, doi:10.1002/qj.49709239103.
- Cifelli, R., C. R. Williams, D. K. Rajopadhyaya, S. K. Avery, K. S. Gage, and P. T. May (2000), Drop-size distribution characteristics in tropical mesoscale convective systems, *J. Appl. Meteorol.*, *39*, 760–777, doi:10.1175/1520-0450(2000)039<0760:DSDCIT>2.0.CO;2.
- Comstock, K. K., S. E. Yuter, R. Wood, and C. S. Bretherton (2007), The three-dimensional structure and kinematics of drizzling stratocumulus, *Mon. Weather Rev.*, *135*, 3767–3784, doi:10.1175/2007MWR1944.1.
- Feingold, G., and Z. Levin (1986), The lognormal fit to raindrop spectra from frontal convective clouds in Israel, *J. Clim. Appl. Meteorol.*, *25*, 1346–1363, doi:10.1175/1520-0450(1986)025<1346:TLFTRS>2.0.CO;2.
- Fox, N. I., and A. J. Illingworth (1997), The potential of a spaceborne cloud radar for the detection of stratocumulus clouds, *J. Appl. Meteorol.*, *36*, 676–687, doi:10.1175/1520-0450-36.6.676.
- Frisch, A. S., C. W. Fairall, and J. B. Snider (1995), Measurement of stratus cloud and drizzle parameters in ASTEX with a K_a -band Doppler radar and a microwave radiometer, *J. Atmos. Sci.*, *52*, 2788–2799, doi:10.1175/1520-0469(1995)052<2788:MOSCAD>2.0.CO;2.
- Frisch, A. S., G. Feingold, C. W. Fairall, T. Uttal, and J. B. Snider (1998), On cloud radar and microwave radiometer measurements of stratus cloud liquid water profiles, *J. Geophys. Res.*, *103*, 23,195–23,197, doi:10.1029/98JD01827.
- Frisch, S., M. Shupe, I. Djalalova, G. Feingold, and M. Poellot (2002), The retrieval of stratus cloud droplet effective radius with cloud radars, *J. Atmos. Oceanic Technol.*, *19*, 835–842, doi:10.1175/1520-0426(2002)019<0835:TROSCD>2.0.CO;2.
- Gage, K. S., C. R. Williams, and W. L. Ecklund (1994), UHF wind profilers: A new tool for diagnosing tropical convective cloud systems, *Bull. Am. Meteorol. Soc.*, *75*, 2289–2294, doi:10.1175/1520-0477(1994)075<2289:UWPANT>2.0.CO;2.
- Giannandrea, S. E., E. P. Luke, and P. Kollias (2010), Automated retrievals of precipitation parameters using non-Rayleigh scattering at 95-GHz, *J. Atmos. Oceanic Technol.*, *27*, 1490–1503, doi:10.1175/2010JTECH1343.1.
- Gossard, E. E. (1994), Measurements of cloud droplet size spectra by Doppler radar, *J. Atmos. Oceanic Technol.*, *11*, 712–726, doi:10.1175/1520-0426(1994)011<0712:MOCDSS>2.0.CO;2.
- Gossard, E. E., J. B. Snider, E. E. Clothiaux, B. Martner, J. S. Gibson, R. A. Kropfli, and A. S. Frisch (1997), The potential of 8-mm radars for remotely sensing cloud drop-size distributions, *J. Atmos. Oceanic Technol.*, *14*, 76–87, doi:10.1175/1520-0426(1997)014<0076:TPOMRF>2.0.CO;2.
- Hildebrand, P. H., and R. S. Sekhon (1974), Objective determination of the noise level in Doppler spectra, *J. Appl. Meteorol.*, *13*, 808–811, doi:10.1175/1520-0450(1974)013<0808:ODOTNL>2.0.CO;2.
- Kollias, P., and B. Albrecht (2010), Vertical velocity statistics in fair weather cumuli at the ARM TWP Nauru climate research facility, *J. Clim.*, *23*, 6590–6604, doi:10.1175/2010JCLI3449.1.
- Kollias, P., B. A. Albrecht, R. Lhermitte, and A. Savtchenko (2001), Radar observations of updrafts, downdrafts, and turbulence in fair-weather cumuli, *J. Atmos. Sci.*, *58*, 1750–1766, doi:10.1175/1520-0469(2001)058<1750:ROOUDA>2.0.CO;2.
- Kollias, P., B. A. Albrecht, and F. Marks Jr. (2002), Why Mie? Accurate observations of vertical air velocities and raindrops using a cloud radar, *Bull. Am. Meteorol. Soc.*, *83*, 1471–1483, doi:10.1175/BAMS-83-10-1471.
- Kollias, P., E. E. Clothiaux, B. A. Albrecht, M. A. Miller, K. P. Moran, and K. L. Johnson (2005), The Atmospheric Radiation Measurement program cloud profiling radars: An evaluation of signal processing and sampling strategies, *J. Atmos. Oceanic Technol.*, *22*, 930–948, doi:10.1175/JTECH1749.1.
- Kollias, P., E. E. Clothiaux, M. A. Miller, E. P. Luke, K. L. Johnson, K. P. Moran, K. B. Widener, and B. A. Albrecht (2007), The Atmospheric Radiation Measurement program cloud profiling radars: Second-generation sampling strategies, processing, and cloud data products, *J. Atmos. Oceanic Technol.*, *24*, 1199–1214, doi:10.1175/JTECH2033.1.
- Krasnov, O. A., and H. W. J. Russenberger (2005), A synergetic radar-lidar technique for the LWC retrieval in water clouds: Description and application to the Cloudnet data, paper presented at 32nd Conference on Radar Meteorology, Am. Meteorol. Soc., Albuquerque, N. M.

- Laury-Micoulaut, C. A. (1976), The n th centred moment of a multiple convolution and its application to an intercloud gas model, *Astron. Astrophys.*, *51*, 343–346.
- Lhermitte, R. M. (1988), Observation of rain at vertical incidence with a 94 GHz Doppler radar: An insight on Mie scattering, *Geophys. Res. Lett.*, *15*, 1125–1128, doi:10.1029/GL015i010p01125.
- Liu, Y., B. Geerts, M. Miller, P. Daum, and R. McGraw (2008), Threshold radar reflectivity for drizzling clouds, *Geophys. Res. Lett.*, *35*, L03807, doi:10.1029/2007GL031201.
- Luke, E. P., P. Kollias, and M. D. Shupe (2010), Detection of supercooled liquid in mixed-phase clouds using radar Doppler spectra, *J. Geophys. Res.*, *115*, D19201, doi:10.1029/2009JD012884.
- Mace, G. G., and K. Sassen (2000), A constrained algorithm for retrieval of stratocumulus cloud properties using solar radiation, microwave radiometer, and millimeter cloud radar data, *J. Geophys. Res.*, *105*, 29,099–29,108, doi:10.1029/2000JD900403.
- Miles, N. L., J. Verlinde, and E. E. Clothiaux (2000), Cloud droplet size distributions in low-level stratiform clouds, *J. Atmos. Sci.*, *57*, 295–311, doi:10.1175/1520-0469(2000)057<0295:CDSIDL>2.0.CO;2.
- Moran, K. P., B. E. Martner, M. J. Post, R. A. Kropfli, D. C. Welsh, and K. B. Widener (1998), An unattended cloud-profiling radar for use in climate research, *Bull. Am. Meteorol. Soc.*, *79*, 443–455, doi:10.1175/1520-0477(1998)079<0443:AUCPRF>2.0.CO;2.
- Nicholls, S. (1984), The dynamics of stratocumulus: Aircraft observations and comparisons with a mixed layer model, *Q. J. R. Meteorol. Soc.*, *110*, 783–820, doi:10.1002/qj.49711046603.
- O'Connor, E. J., R. J. Hogan, and A. J. Illingworth (2005), Retrieving stratocumulus drizzle parameters using Doppler radar and lidar, *J. Appl. Meteorol.*, *44*, 14–27, doi:10.1175/JAM-2181.1.
- Pincus, R., and M. B. Baker (1994), Effect of precipitation on the albedo susceptibility of clouds in the marine boundary layer, *Nature*, *372*, 250–252, doi:10.1038/372250a0.
- Randall, D. A., J. A. Coakley Jr., D. H. Lenschow, C. W. Fairall, and R. A. Kropfli (1984), Outlook for research on subtropical marine stratiform clouds, *Bull. Am. Meteorol. Soc.*, *65*, 1290–1301, doi:10.1175/1520-0477(1984)065<1290:OFROSM>2.0.CO;2.
- Rogers, R. R., and R. J. Pilié (1962), Radar measurements of drop-size distribution, *J. Atmos. Sci.*, *19*, 503–506, doi:10.1175/1520-0469(1962)019<0503:RMODSD>2.0.CO;2.
- Rogers, R. R., and M. K. Yau (1989), *A Short Course in Cloud Physics*, 3rd ed., 290 pp., Elsevier, New York.
- Rogers, R. R., W. L. Ecklund, D. A. Carter, K. S. Gage, and S. A. Ethier (1993), Research applications of a boundary layer wind profiler, *Bull. Am. Meteorol. Soc.*, *74*, 567–580, doi:10.1175/1520-0477(1993)074<0567:RAOABL>2.0.CO;2.
- Sauvageot, H., and J. Omar (1987), Radar reflectivity of cumulus clouds, *J. Atmos. Oceanic Technol.*, *4*, 264–272, doi:10.1175/1520-0426(1987)004<0264:RROCC>2.0.CO;2.
- Serpetzoglou, E., B. Albrecht, P. Kollias, and C. W. Fairall (2008), Boundary layer, cloud, and drizzle variability in the southeast Pacific stratocumulus regime, *J. Clim.*, *21*, 6191–6214, doi:10.1175/2008JCLI2186.1.
- Shupe, M. D., P. Kollias, S. Y. Matrosov, and T. L. Schneider (2004), Deriving mixed-phase cloud properties from Doppler radar spectra, *J. Atmos. Oceanic Technol.*, *21*, 660–670, doi:10.1175/1520-0426(2004)021<0660:DMCPFD>2.0.CO;2.
- Stevens, B., W. R. Cotton, G. Feingold, and C.-H. Moeng (1998), Large-eddy simulations of strongly precipitating, shallow, stratocumulus-topped boundary layers, *J. Atmos. Sci.*, *55*, 3616–3638, doi:10.1175/1520-0469(1998)055<3616:LESOSP>2.0.CO;2.
- vanZanten, M. C., and B. Stevens (2005), Observations of the structure of heavily precipitating marine stratocumulus, *J. Atmos. Sci.*, *62*, 4327–4342, doi:10.1175/JAS3611.1.
- Wakasugi, K., A. Mizutani, M. Matsuo, S. Fukao, and S. Kato (1986), A direct method for deriving drop-size distribution and vertical air velocities from VHF Doppler radar spectra, *J. Atmos. Oceanic Technol.*, *3*, 623–629, doi:10.1175/1520-0426(1986)003<0623:ADMFD>2.0.CO;2.
- Wakasugi, K., A. Mizutani, M. Matsuo, S. Fukao, and S. Kato (1987), Further discussion on deriving drop-size distributions and vertical air motions directly from VHF Doppler radar spectra, *J. Atmos. Oceanic Technol.*, *4*, 170–179, doi:10.1175/1520-0426(1987)004<0170:FDODDS>2.0.CO;2.
- Wang, J. Y., and B. Geerts (2003), Identifying drizzle within marine stratus with W-band radar reflectivity profiles, *Atmos. Res.*, *69*, 1–27, doi:10.1016/j.atmosres.2003.08.001.
- Widener, K., and J. Mead (2004), W-band ARM cloud radar—specification and design, paper presented at Fourteenth ARM Science Team Meeting, U.S. Dep. of Energy, Albuquerque, N. M.
- Williams, C. R., W. L. Ecklund, and K. S. Gage (1995), Classification of precipitating clouds in the Tropics using 915-MHz wind profilers, *J. Atmos. Oceanic Technol.*, *12*, 996–1012, doi:10.1175/1520-0426(1995)012<0996:COPCIT>2.0.CO;2.
- Zrníc, D. S. (1975), Simulation of weatherlike Doppler spectra and signals, *J. Appl. Meteorol.*, *14*, 619–620, doi:10.1175/1520-0450(1975)014<0619:SOWDSA>2.0.CO;2.

P. Kollias, J. Rémillard, and W. Szyrmer, Department of Atmospheric and Oceanic Sciences, McGill University, Burnside Hall, Rm. 945, 805 Sherbrooke St. W., Montreal, QC H3A 2K6, Canada. (pavlos.kollias@mcgill.ca)

E. Luke, Atmospheric Sciences Division, Brookhaven National Laboratory, Bldg. 490D, Bell Avenue, Upton, NY 11973, USA.